Molecular Systems Biology 6; Article number 396; doi:10.1038/msb.2010.49
Citation: ***Molecular Systems Biology*** **6:396**

www.molecularsystemsbiology.com

molecular systems biology

REPORT

Systems parasitology: effects of *Fasciola hepatica* on the neurochemical profile in the rat brain

Jasmina Saric[1,2,8,*], Jia V Li[1,2,8], Jürg Utzinger[2,3], Yulan Wang[4], Jennifer Keiser[3,5], Stephan Dirnhofer[6], Olaf Beckonert[1], Mansour TA Sharabiani[7], Judith M Fonville[1], Jeremy K Nicholson[1] and Elaine Holmes[1,*]

[1] Biomolecular Medicine, Department of Surgery and Cancer, Faculty of Medicine, Imperial College London, London, UK, [2] Department of Epidemiology and Public Health, Swiss Tropical and Public Health Institute, Basel, Switzerland, [3] University of Basel, Basel, Switzerland, [4] State Key Laboratory of Magnetic Resonance and Atomic and Molecular Physics, Wuhan Center for Magnetic Resonance, Wuhan Institute of Physics and Mathematics, Chinese Academy of Sciences, Wuhan, People's Republic of China, [5] Department of Medical Parasitology and Infection Biology, Swiss Tropical and Public Health Institute, Basel, Switzerland, [6] Institute of Pathology, University Hospital Basel, Basel, Switzerland and [7] Department of Epidemiology and Biostatistics, School of Public Health, Faculty of Medicine, Imperial College London, London, UK
[8] These authors contributed equally to this work
* Corresponding authors. J Saric or E Holmes, Biomolecular Medicine, Department of Surgery and Cancer, Faculty of Medicine, Imperial College London, Sir Alexander Fleming Building, South Kensington, London SW7 2AZ, UK. Tel.: +44 20 7594 3899; Fax: +44 20 7595 3221; E-mail: jasmina.saric@imperial.ac.uk or Tel.: +44 20 7594 3220; Fax: +44 20 7595 3221; E-mail: elaine.holmes@imperial.ac.uk

Received 5.2.10; accepted 31.5.10

We characterize the integrated response of a rat host to the liver fluke *Fasciola hepatica* using a combination of ^{1}H nuclear magnetic resonance spectroscopic profiles (liver, kidney, intestine, brain, spleen, plasma, urine, feces) and multiplex cytokine markers of systemic inflammation. Multivariate mathematical models were built to describe the main features of the infection at the systems level. In addition to the expected modulation of hepatic choline and energy metabolism, we found significant perturbations of the nucleotide balance in the brain, together with increased plasma IL-13, suggesting a shift toward modulation of immune reactions to minimize inflammatory damage, which may favor the co-existence of the parasite in the host. Subsequent analysis of brain extracts from other trematode infection models (i.e. *Schistosoma mansoni*, and *Echinostoma caproni*) did not elicit a change in neural nucleotide levels, indicating that the neural effects of *F. hepatica* infection are specific. We propose that the topographically extended response to invasion of the host as characterized by the modulated global metabolic phenotype is stratified across several bio-organizational levels and reflects the direct manipulation of host–nucleotide balance.
Molecular Systems Biology **6**: 396; published online 27 July 2010; doi:10.1038/msb.2010.49
Subject Categories: cellular metabolism; molecular biology of disease
Keywords: brain; *Fasciola hepatica*; immunology; metabolic profiling; nuclear magnetic resonance spectroscopy

Introduction

Fascioliasis is a re-emerging zoonotic disease caused by two liver fluke species, *Fasciola hepatica* and *F. gigantica*. As many as 17 million people might be infected with *Fasciola* spp. (Keiser and Utzinger, 2009) and the disease is of considerable economic and public health importance. At present, triclabendazole is the only drug available for treatment of infected human beings and livestock and worryingly, parasite resistance to triclabendazole is already widespread in farm animals (Fairweather, 2009). Hence, a deeper understanding of the biology of this parasite is warranted to uncover novel therapeutic targets. Fundamental investigations in well-controlled host–parasite models hold promise for recovery of metabolic biomarkers, at different bio-organizational levels. This may promote the mechanistic understanding of the host response to infection at the systems level with a view to identifying drug targets.

The regulation of any mammalian system is such that events originating in a discrete tissue or organ can trigger a cascade of consequent events throughout the host system as the host attempts to maintain homeostatic equilibrium (Lederberg,

2000; Nicholson *et al*, 2002). Thus, the effects of a parasitic infection are rarely confined to a single target tissue; instead a network of molecular events can generally be detected throughout the host system. Top-down systems biology driven by metabolic phenotyping and metabonomics (Nicholson *et al*, 1999; Holmes *et al*, 2008a; Li *et al*, 2008a, b; Tsang *et al*, 2009) has been shown to be a useful tool for studying host–parasite (Saric *et al*, 2008; Wang *et al*, 2008; Li *et al*, 2009) and host–symbiont interactions (Nicholson *et al*, 2005; Martin *et al*, 2007; Holmes *et al*, 2008b), and it is clear that any transgenomic interaction can only be studied *in vivo*, as the effects of microbial or parasitic modulations are panorganismal (Wang *et al*, 2008; Saric *et al*, 2009).

In this study, we characterize and interpret the system-wide effect of *F. hepatica* in the rat, using a metabolic profiling strategy to develop mechanistic hypotheses. A multilevel statistical approach was applied to the analysis of ^{1}H nuclear magnetic resonance (NMR) spectroscopy-generated data to obtain an integrative profile of the global response of the host based on differential metabolic, immunological, and biometric responses across multiple tissues. We report novel findings regarding the effect of *F. hepatica* on the neural metabolite profile of the rat and show metabolic connections between the liver, gut, and brain, which we compare with the metabolic effects elicited by two separately assessed trematode infections, namely *Schistosoma mansoni* and *Echinostoma caproni* in a mouse model. Although *F. hepatica*-induced liver damage has been described in detail before (Lim *et al*, 2007; Marcos *et al*, 2008), no direct association with the central nervous system has been found in the extant literature. The findings from this study expose a potential mechanism of parasite-induced immune modulation and exemplify the value of top-down systems approaches based on metabolic profiling for recovering mechanistic information from a system without *a priori* knowledge.

Results and discussion

Parasite burden, physiological monitoring, and histology

Patent infection of rats with *F. hepatica* resulted in a mean parasite burden of 5.5 (range=2–10; s.d.=2.6) on day 77 postinfection and a significant reduction of the mean packed cell volume (PCV) at day 71 postinfection (uninfected control rats: mean=50.8%, s.d.=2.8%; infected: mean=42.0%, s.d.=3.8%). The mean bodyweight did not significantly differ between infected and uninfected rats at any of the investigated time points. Clear evidence of hepatic necrosis was found in *F. hepatica*-infected rats (Supplementary Figure S1) together with follicular hyperplasia of splenic white pulp and interstitial lymphoplasmocytic inflammatory infiltrates in the kidney.

Multivariate statistical modeling of *F. hepatica* infection

Assignment of metabolic components in the tissues and biofluid profiles for both uninfected and infected rats were made on the basis of extant literature (Coen *et al*, 2003; Holmes *et al*, 2006; Beckonert *et al*, 2007; Li *et al*, 2009; Saric *et al*, 2009; Tsang *et al*, 2009), and in the case of the brain extract spectra, from addition of authentic standards (assignments provided in Supplementary Figure S2; Supplementary Table SI).

The metabolic changes in the rat caused by patent infection with *F. hepatica* were modeled separately for each biological matrix through principal component analysis (PCA) and projection to latent structure discriminant analysis (PLS-DA). In brief, the metabolic profiles of *F. hepatica*-infected rats could be differentiated from those of uninfected control rats through PCA for all assessed biological compartments except the ileum and the renal medulla. A list of important infection-discriminatory metabolites is given in Table I together with the *P*-values, validated by permutation testing, Figure 1.

Consistent changes in lipid metabolism, including elevated choline and/or choline derivatives such as betaine, phosphocholine, and glycerophosphocholine (GPC) occurred throughout most tissues (Figure 1; Table I). This indicates a generally increased usage of choline-derived metabolites that can be further converted to phosphocholine (Zeisel *et al*, 2003; Li and Vance, 2008), a basic component of membrane anabolism, or used for the production of polyunsaturated fatty acids such as arachidonic acid, which gives rise to pro-inflammatory eicosanoic mediators (Calder, 2008, 2009). Prostaglandins, for instance, exert multiple pro-inflammatory effects, such as chemotaxis of neutrophils, which are typically the first infiltrating cells at sites of tissue damage. Evidence of inflammatory infiltrates was detected in the histological and metabolic profiles of the liver, spleen, and kidney (Supplementary Figure S1) and inflammation was implicated biochemically in the colon and plasma. Increased plasma intensities of *O*- and *N*-acetyl glycoprotein signals were noted in *F. hepatica*-infected rats. Increased concentrations of acetylated glycoproteins have been earlier identified in *Trichinella spiralis*- and *Trypanosoma brucei brucei*-infected mice (Martin *et al*, 2006; Wang *et al*, 2008) as inflammatory markers and include acute phase reaction proteins, such as α1 acid glycoprotein, haptoglobin, and transferrin, which are produced in the liver and which show markedly increased serum levels during such systemic responses to inflammation (Schreiber *et al*, 1982; Bell *et al*, 1987a, b) (Figure 1; Table I).

Other features of *F. hepatica* infection were specific to a single biological compartment; for example hippurate, which is only observed in the urine, was found to be decreased in infected rats, reflecting a parasite-induced disturbance of the gut-microbial composition or activity (Nicholls *et al*, 2003; Li *et al*, 2008a, b). The liver, spleen and plasma showed the greatest changes at the low molecular weight level, consistent with the direct damage caused by the migrating larvae of *F. hepatica* during the acute stage of an infection in the hepatic tissue and the immunological activity in the spleen (Supplementary Figure S1). The proliferation of B cells in the spleen primary follicles as response to blood-borne antigens uses amino acids and lipid fractions for the new cellular membrane bilayers and organelles and may account for the major changes in the metabolic profile of the spleen, and perhaps in other tissue compartments. The depletion in hepatic glucose is more likely to be related to the direct damage of the energy stores and is consistent with elevated glucose levels in plasma.

Table I Candidate biomarkers extracted through O-PLS-DA of *F. hepatica*-infected and uninfected rats within selected tissue compartments

	pl	ur	fw	li	sp	rc	je	co		pl	ur	fw	li	sp	rc	je	co
3-methyl-2-oxovalerate			0.004						leucine					0.004	0.001	0,015	
α-aminoadipate		*			*				*myo*-inositol						0.010		0.010
2-ketoglutarate	0.003								*N*-acetyl glycoproteins	*							
betaine	*				*	0.007			*O*-acetyl glycoproteins	0.002							
butyrate			0.007						phenylalanine				0.042			*	0.003
bile acids		0.002							phosphocholine				0.049		0.013		
choline				0.015	*	*		0.002	taurine							0.010	
creatine							0.018		trimethylamine-*N*-oxide	*							
creatinine		0.008							tyrosine				0.001			0.003	0.009
fumarate							0.003		valine					0.005		0,001	0.013
glucose	0.011		0.002	0.008	*				lipid term CH_3	0.001							0.004
glutamate				0.003					lipid $(CH_2)n$			*					0.004
glycerophosphocholine				0.030	0.013	0.002		0.012	lipid ($\mathbf{CH_2}CH_2CO$)	0.018							0.003
glycogen				*					lipid ($CH_2C{=}C$)								0.002
hippurate		0.017							lipid (CHOCOR)				*				
inosine							0.010		lipid ($CH_2\mathbf{CH_2}CO$)	0.016							0.003
isoleucine					*		0.003		lipid (=CH-$\mathbf{CH_2}$-CH=)								0.002
lactate					*	*			lipid (CH=CH)								0.003

pl, plasma; ur, urine; fw, fecal water; li, liver; sp, spleen; rc, renal cortex; je, jejenum; co, colon; red: relatively increased; blue: decreased levels caused by infection with *F. hepatica;* * <0.001.
Corresponding *P*-values are listed.

One of the strongest effects of infection with *F. hepatica* manifested in the neurochemical profiles, further highlighting the ability of the parasite to impact on remote tissue. Clear visual separation of the infected and uninfected animals was achieved in the PCA and PLS-DA scores plots (Figure 2A and B) of the neural profiles, with a model predictivity (Q^2Y) of 0.46. The pattern of differentiating metabolites in the neurochemical profiles as extracted from the orthogonal PLS-DA (O-PLS-DA) coefficients was composed of a significant increase in the relative levels of inosine, tyrosine, and phenylalanine. Conversely, the relative tissue concentrations of GPC, succinate, inosine mono-, di-, and triphosphate, adenosine, and adenosine mono-, di-, and triphosphate were lower in the brains of infected animals (Figure 2C and D).

Secretion of nucleotide-degrading enzymes occurs in a variety of ecto- and endoparasitic organisms, such as ticks, blood sucking insects, and helminths and serves the primary purpose of minimizing immune reactions in the host organism to prolong their survival (Parshad and Guraya, 1977; Ribeiro and Francischetti, 2003). For example, adenosine deaminase and 5′-nucleotidase have been found in secretory channels of *T. spiralis* and *F. gigantica* (Gounaris, 2002; Ali, 2008). The former catalyzes the intracellular conversion of adenosine to inosine, whereas the latter hydrolyzes inosine monophosphate (Figure 2E).

We observed a substantial shift of adenosine and phosphorylated nucleotides to inosine in the host brain, which indicates an attenuated inflammatory response and may be suggestive that *F. hepatica*, similarly to *F. gigantica*, secretes nucleotide-degrading enzymes. Both inosine and adenosine induce mast cell degranulation, an event that has a central function in localized inflammatory response, an important mediator of type I hypersensitivity reactions, with adenosine being the more potent activator (Marquardt *et al*, 1978; Tilley *et al*, 2000). Furthermore, inosine, which was believed to be inert for a long time, has been proven to effectively suppress pro-inflammatory cytokines such as IFN-γ, TNF-α, and IL-12 (Hasko *et al*, 2000, 2004; Mabley *et al*, 2003) *in vitro* and *in vivo*.

We assessed the concentrations of selected plasma cytokines and found the levels of both IL-13 and IL-5 to be significantly higher in *F. hepatica*-infected rats compared with the control group on day 22 postinfection. IL-13 maintained a significant increase on day 43 postinfection (Figure 2E). An enhanced Th2 immune response such as that suggested by the increase in both IL-5 and IL-13 would serve to counteract mechanisms of inflammation. IL-13 is also an important direct negative regulator of inflammatory cytokines in macrophages (Minty *et al*, 1993). Minimization of such an intense immune reaction, and hence prolongation of the period in which the parasite can remain undetected by the host at earlier stages of infection, is clearly beneficial for the survival of the worms.

Comparison of the systemic effects of *F. hepatica* with *S. mansoni* and *E. caproni*

To ascertain the specificity of the global metabolic response of the rat to *F. hepatica* across different tissue compartments, particularly with respect to the observed modulation of the neural nucleotide balance, two further rodent-trematode models were compared, namely *S. mansoni* and *E. caproni*, in a murine host. Both trematodes induced a biochemical response across a range of biological compartments, but whereas *S. mansoni* caused pathology in the spleen and liver (Li *et al*, 2009), no overt necrosis was found in any tissue after *E. caproni* infection (Saric *et al*, 2009). At a global level, *E. caproni* infection was predominantly characterized by

malabsorption of amino acids, which manifested predominantly in the biochemical profiles of the small intestine and liver. Altered amino-acid levels and energy metabolism were also a core signature of *S. mansoni* infection with disturbed levels of choline-containing membrane components in the liver and intestinal tissues.

As the altered neural nucleotide signature was one of the strongest metabolic responses in rats infected with *F. hepatica*, we directly compared the metabolic profiles of brain extracts with those from *S. mansoni* and *E. caproni* in the mouse. *S. mansoni* infection induced obvious changes in the metabolic composition of the host brain, as indicated by the PCA and PLS-DA scores plots (Supplementary Figure S3), with the PLS-DA model indicating a predictive value (Q^2Y) of 0.61. Infection with *S. mansoni* was characterized by higher levels of glutamine, but lower concentrations of γ-aminobutyric acid (GABA), choline, phosphocholine, and *scyllo*-inositol (Supplementary Figure S3C). The *E. caproni*-infected animals could not be statistically differentiated from the corresponding control group based on the brain extract spectra ($Q^2Y=-0.21$, data not shown), indicating that the infection did not systematically alter the brain biochemistry of the host.

Although both *S. mansoni* and *F. hepatica* induced a marked perturbation of the neurochemical profiles in their host animals, the patterns of differentiating metabolites were distinct for these two trematode-rodent models, with the exception of the common effect of decreasing concentrations of lipid degradation products, such as choline, phosphocholine, and GPC, all of which have a function in cell membrane formation. In contrast to the perturbed immunological function suggested by the altered nucleotide levels in the brains of *F. hepatica*-infected animals, modulation of the neural metabolite profile by *S. mansoni* infection suggested the dominant effect related to the neurotransmitters, as supported by depleted levels of GABA and increased tissue concentrations of glutamine, which is a substrate for both excitatory and inhibitory neurotransmitters, including GABA. However, as neural GABA decreased in infected animals, the increased concentrations of glutamine are more likely to be indicative of a detoxification process. Compensatory locations for ammonium detoxification are muscle cells and the brain, combining ammonia and glutamate to glutamine (Kreis *et al*, 1991; Olde Damink *et al*, 2002), which could also contribute to the relatively higher levels of glutamine in the brain extracts of *S. mansoni*-infected mice documented in the current investigation.

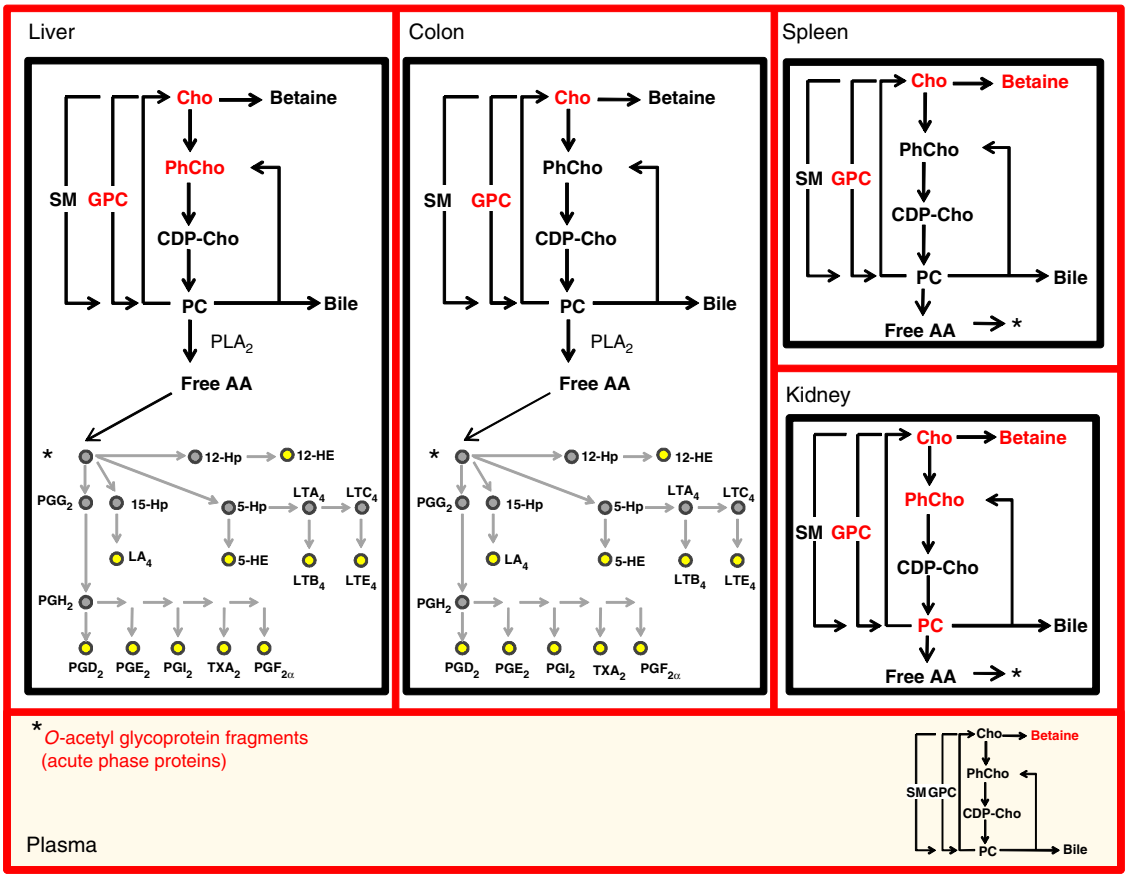

Figure 1 Summary of the systemic involvement of choline-containing species and their potential relationship with inflammatory processes. Increased immune activity in the liver- and gut-associated lymphoid tissue (GALT) in the colon on *F. hepatica* infection may lead to cell-internal lipid degradation to arachidonic acid, which is the substrate of many eicosanoic pro-inflammatory mediators. The spleen and the kidney, in which inflammatory activity is less extensive, respond to the infection with increased betaine, which shares the same pathway. AA, amino acids; CDP-Cho, CDP-choline; Cho, choline; GPC, glycerophosphocholine; HE, hydroxyeicosatetraenoic acid; Hp, hydroxyperoxy-eicosatetranoic acid; LA, lipoxin; LT, leukotrienes; PC, phosphatidylcholine; PG, prostaglandine; PhCho, phosphocholine; PL, phospholipase; SM, sphingomyelin; TX, thromboxane; red; increased relative metabolic levels; *pro-inflammatory effects.

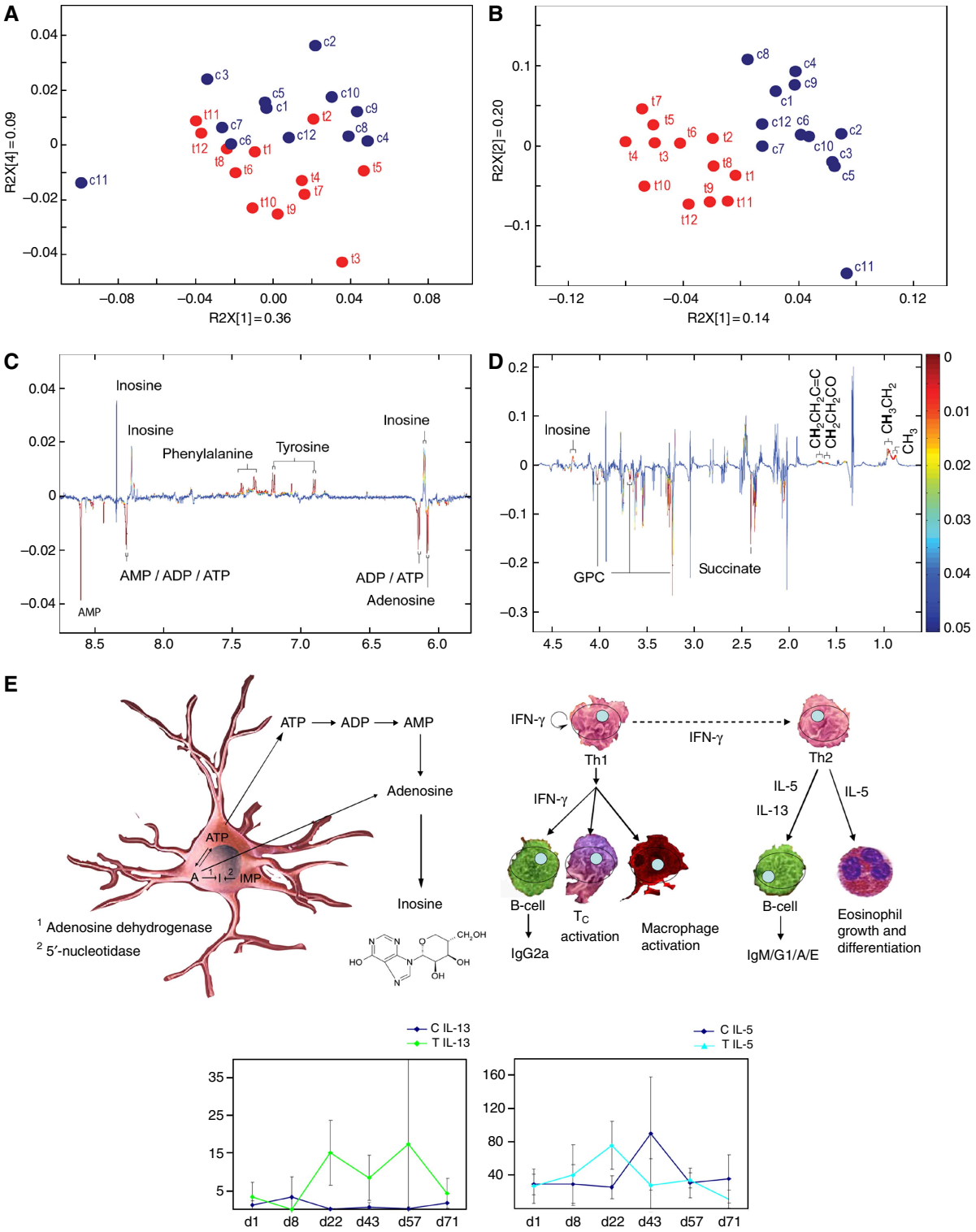

Figure 2 Multivariate analysis of brain spectra from the *F. hepatica*-rat infection model. (**A**) PCA scores plot and (**B**) PLS-DA scores plot showing differences between *F. hepatica*-infected (red; c1–c12) and uninfected animals (blue; t1–t12). *P*-value back projection to O-PLS-DA analysis of *F. hepatica*-infected (upward oriented peaks) and uninfected animals (downward oriented peaks) for the aliphatic region (**C**) and aromatic region (**D**), whereby the metabolic regions differentiating between infected and uninfected animals ($P < 0.05$) are color coded according to the power of discrimination. (**E**) Schematic of intra- and extracellular adenosine–inosine interconversion in the brain by two main enzymes, [1]adenosine dehydrogenase and [2]5′-nucleotidase. The shift from adenosine toward inosine observed in the coefficient plots in (C) and (D) may lead to emphasized Th2-mediated immune mechanisms reflected by increased levels of IL-5 and, IL-13. Plasma cytokine assessment on days 1, 8, 22, 43, 57 and 71 (d) post-infection confirmed significantly higher levels of IL-5 and IL-13 in the *F. hepatica*-infected animals (cyan and green, respectively) at day 22 postinfection in the case of IL-5, and days 22 and 43 postinfection for IL-13, compared with the uninfected animals (blue). A, adenosine; I, inosine.

Systems impact of the modulation of the neural metabolic phenotype of *F. hepatica* infection: multivariate modeling and integration of physiological compartments

Metabolic correlates of the six important discriminatory spectral regions containing inosine, GPC, succinate, tyrosine, phenylalanine, and the overlapped regions containing adenosine and the phosphorylated nucleotides in the brain tissue of *F. hepatica*-infected rats were identified in each of the other tissue or biofluid matrices. Sequential correlations between the integrated-discriminatory signals in the brain spectra tissue were made with the whole spectra from each tissue and with the spectra from biofluids obtained at day 71 postinfection (Figure 3; Supplementary Table SII). Here, univariate correlation of single signals was preferred over a multivariate approach to maximize information recovery and to infer direct inter-compartmental links between the metabolites. A comprehensive list of compartment-specific correlations with the neural metabolites is provided in Supplementary Table SII. The liver, urine, and spleen showed the highest number of components correlated with the selected brain metabolites. The high degree of correlation between the metabolic markers in the brain and the liver spectra across the tissue compartments (Figure 3A) may simply relate to the magnitude of spectral changes in both organs and does not necessarily imply any causal relationships between metabolites. The gross changes in the hepatic metabolite profile are reflective of direct mechanical damage of the liver tissue by the migration and feeding of the juvenile fluke, whereas the effect of the parasite on remote organs such as the brain is more difficult to rationalize. Hepatic dysfunction in *F. hepatica* infection is known to result in increased circulating toxins, such as ammonia, thiols, and phenols (Zaki *et al*, 1983), which are typically released after hepatic failure, because of reduced ability to degrade aromatic amino acids and ammonia. Animals infected with *F. hepatica* showed increased neural concentrations of phenylalanine and tyrosine. Indeed, it has been shown that hepatic failure induces an increased passive permeability of the blood–brain barrier for several substances, among which phenylalanine and tyrosine were found to increase up to 30% in the host brain (Zaki *et al*, 1984).

A recurrent theme across multiple levels of this host–parasite system was the inflammatory response, which manifested at both the level of structural damage and that of the metabolite signature. The increased signal intensities of plasma acetyl glycoprotein fragments were statistically associated with all six cerebral markers of infection underscoring the presence and global effect of a strong infection-induced inflammatory response (Figure 3B; Supplementary Table SII). Interestingly, a shift has been observed in the brain nucleotides inosine and adenosine in favor of inosine, which has been shown to have anti-inflammatory effects at the posttranscriptional level (Hasko *et al*, 2000), including suppression of pro-inflammatory cytokines (e.g. IFN-γ and TNF-α) and minimizing macrophage-mediated mechanisms of inflammation (Hasko *et al*, 2000, 2004; Liaudet *et al*, 2002). This shift may be directly induced by nucleotide-degrading secretory enzymes of *F. hepatica*. Significant direct correlations between the selected neural indices of *F. hepatica* infection and compounds involved in lipid metabolism were detected.

In addition to the correlations driven by the liver pathology, direct metabolic interactions such as plasma glucose being anti-correlated with brain succinate and 2-ketoglutarate, suggestive of an interaction through glycolysis and the tricarboxylic acid cycle, were found. Another example of such co-variation is the inverse correlation between cerebral tyrosine and urinary hippurate, deriving from gut-microbial/mammalian co-metabolism. Direct alteration of urinary metabolite signatures through gut-microbial species seems to be a common feature of many host–parasite models (Martin *et al*, 2006; Li *et al*, 2008a; Saric *et al*, 2008; Wang *et al*, 2008). Here, the negative correlations of cerebral adenosine with urinary dimethylglycine and the bile acids, which are co-metabolized by gut microbiota, strengthens the notion of a bidirectional communication between gut and brain (gut–brain axis). This leads to the hypothesis that nucleotide-initiated immunoactivity has a function in the changed gut-microbial dynamics observed in parasitic infections.

In conclusion, we have characterized the global metabolic phenotype of a host–parasite system and have shown a clear effect of a trematode infection on the biochemical composition of the host brain using a metabolic profiling strategy to develop and pursue hypotheses relating to the observed neurochemical changes in the rat. *F. hepatica* induced a focussed response, primarily associated with the hypothesized worm-induced shift from adenosine toward inosine and the subsequent induction of anti-inflammatory cytokines. The coherence of the histological, metabolic, and cytokine data further facilitated elucidation of general and specific metabolic events and provided a means of probing inter-compartmental co-variation of metabolites. Thus, the application of a top-down systems approach has been shown to be of value in driving the articulation of novel mechanistic hypotheses relating to parasitic invasion and has wide application in molecular parasitology.

Materials and methods

F. hepatica-rat model and experimental design

Experimental procedures were carried out at the Swiss Tropical and Public Health Institute (Swiss TPH; Basel, Switzerland), adhering to local and national guidelines of animal welfare (permission no. 2070 and 2081). A total of 24 Wistar female rats were purchased from RCC (Itingen, Switzerland) and kept under environmentally controlled conditions (temperature: 25°C; relative humidity: 60–70%; light/dark cycle: 12/12 h). Rats were acclimatized for 1 week and all animals had free access to commercially available rodent diet obtained from Nafag (Gossau, Switzerland) and community tap water.

Rats were individually marked and group housed with four animals per cage. Twelve rats were orally infected with 20–25 *F. hepatica* metacercariae each (Cullompton isolate) obtained from Mr G Graham (Addleston, UK). The remaining 12 rats were left uninfected and served as controls.

The body weight of each animal was measured throughout the experiment. On day 1 pre-infection and days 1, 4, 8, 15, 22, 28, 36, 43, 57, and 71 postinfection, urine and feces were collected into Petri dishes by rubbing the abdomen of the rats gently. Approximately 50 µl of blood was collected from the tail tips collected into hematocrit capillaries (Sodium [Na] heparin coated) and spun at 10 500 *g* for 4 min. The PCV was calculated and expressed as a percentage of the plasma ratio to red blood cells (Li *et al*, 2008a).

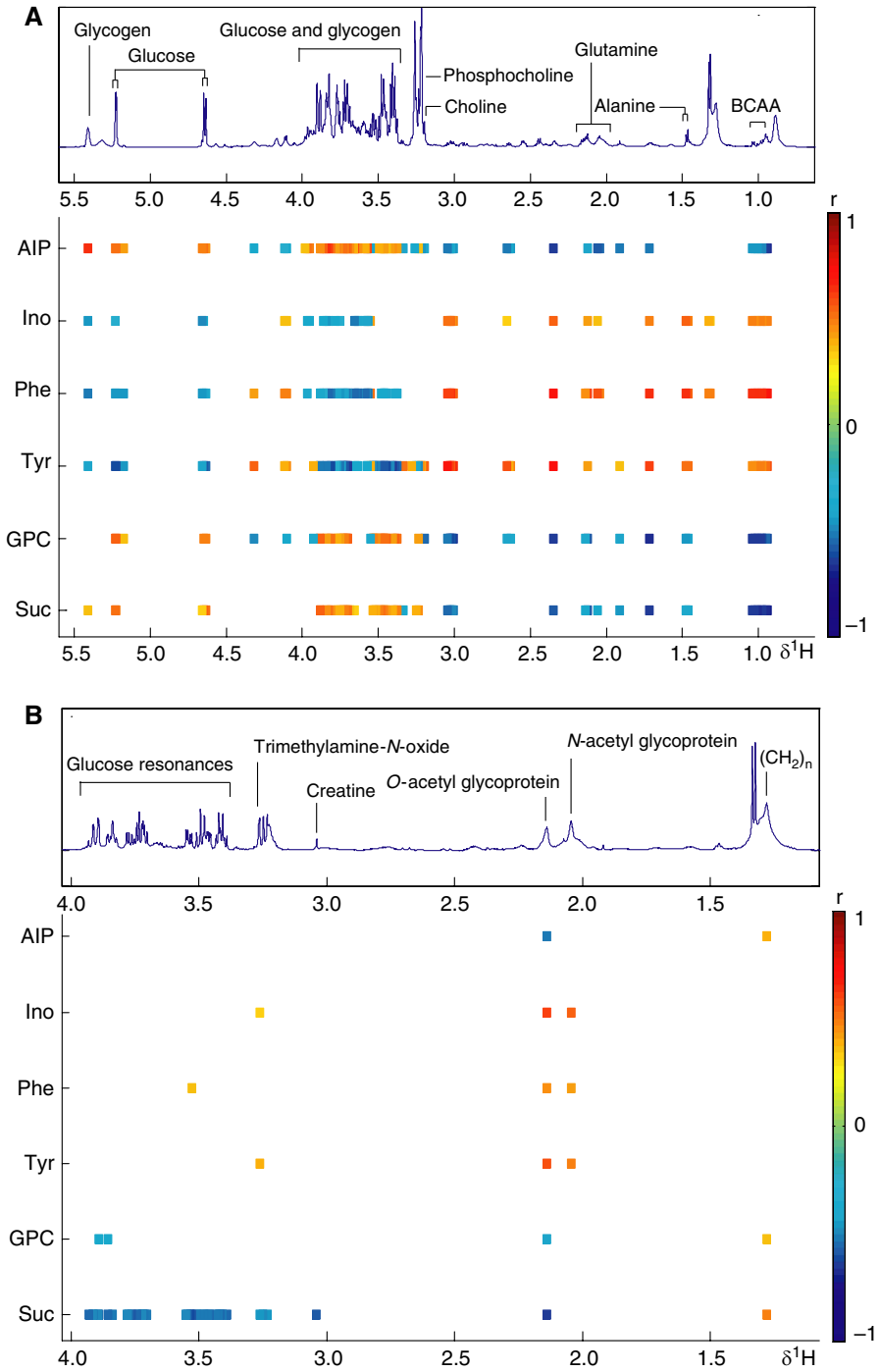

Figure 3 Correlation plots showing significant associations between the ^{1}H NMR spectra of (**A**) liver and (**B**) plasma each as the *X*-matrix with the integrals of the control/infection-differentiating metabolites of the brain extracts (AIP, adenosine and phosphorylated nucleotides; BCAA, branched chain amino acids; GPC, glycerophosphocholine; Ino, inosine; Phe, phenyalanine; Suc, succinate; Tyr, tyrosine) as the *Y*-matrix are color coded according to the correlation coefficient.

All animals were euthanized on day 77 postinfection using CO_2, and the worm burden was determined in each infected animal by removing adult flukes from the livers and bile ducts on dissection. The whole brains of rats, regardless of their infection status, were removed on dissection and the left hemispheres were transferred into cryo-tubes, snap frozen in liquid nitrogen and stored at −80°C pending ^{1}H NMR spectroscopic data acquisition. In addition, the left lateral lobe of the liver, the left kidney, spleen, and three parts of the intestine (colon, ileum, and jejunum) were removed and stored in the same manner as the brain for ^{1}H NMR spectroscopic data acquisition. The right brain hemispheres, the right kidney, and parts of the spleen, liver, and intestines were transferred into separate Eppendorf tubes containing 4% buffered formalin for subsequent histological examination.

Methodology relating to the *S. mansoni*- and *E. caproni*-mouse models has been described earlier (Saric *et al*, 2008, 2009; Li *et al*, 2009) and followed a similar protocol to that described for *F. hepatica* infection in the rat.

Sample preparation for ^{1}H NMR spectroscopy

Each brain sample was placed in a mortar, mashed using a 1 ml mixture of H_2O and acetonitrile (1:1, v:v) and transferred into a glass tube. Another 2 ml of the solvent mixture was used to rinse the mortar twice and transferred into the same glass tube. The brain homogenate was centrifuged for 6 min at 10 000 *g*. The supernatant was collected into a new glass vial, evaporated overnight and lyophilized. The resultant dry mass was resuspended into 0.55 ml of D_2O until completely dissolved and transferred into a 5 mm-outer-diameter NMR tube for subsequent analyses. Urine, plasma, and fecal pellets were prepared for conventional high-resolution ^{1}H NMR data acquisition as described earlier (Saric *et al*, 2008), whereas tissue metabolic fingerprints were acquired through magic angle spinning (MAS) ^{1}H NMR (Saric *et al*, 2009).

The extraction protocol for the *S. mansoni*-mouse model was slightly extended to gain additional information regarding potential changes in the lipid metabolic profile, as a pharmacological intervention was involved in the original study protocol. Each brain sample obtained from mice infected with *S. mansoni* and the corresponding uninfected control mice was transferred into a 2 ml Eppendorf tube containing a metal bead, 0.75 ml of water, and 0.75 ml of methanol. The Eppendorf tube was placed in the tissue lyser and shaken for 5 min at the speed of 22 Hz. The resulting brain homogenate was transferred into a glass tube. A further 0.75 ml of each liquid was used to rinse the Eppendorf tube and transferred into the same glass tube. A total of 1.5 ml of chloroform was added into the mixture and centrifuged at 2500 *g* for 30 min. The aqueous and the chloroform phases were transferred into a new glass tube each and both were left to evaporate overnight and lyophilized. Before ^{1}H NMR analysis, the powder obtained from the aqueous phase was dissolved in 0.55 ml phosphate buffer (D_2O:H_2O=9:1, v:v, 0.01 % of sodium 3-(trimethylsilyl) propionate-2,2,3,3-d4 ([TSP)], pH=7.4), whereas the dry mass of the chloroform fraction was dissolved in deuterated chloroform ($CDCl_3$).

Acquisition of ^{1}H NMR spectral data

All ^{1}H NMR spectra from rat and mouse brain extracts, urine, plasma, and fecal water were recorded on a Bruker Avance 600 NMR spectrometer (Bruker; Rheinstetten, Germany), operating at 600.13 MHz for proton frequency. A 5-mm triple resonance probe with inverse detection for proton frequency was used (Bruker), using a standard one-dimensional NMR experiment with pulse sequence (recycle delay (RD)-90°-t_1-90°-t_m-90°-acquisition time). Optimal water suppression was achieved by irradiating the water frequency during the RD set to 2 s and the mixing time of 100 ms. The 90° pulse length was adjusted to 10.62 μs for the brain extracts of both the *F. hepatica* rat and the *E. caproni*-mouse models and 13.5 μs for the *S. mansoni*-mouse model. A total of 128 scans were acquired for each sample into 32k data points using a spectral width of 20 p.p.m. All free induction decays were multiplied by an exponential function equivalent to a 0.3 Hz line-broadening factor before Fourier transformation. Liver, spleen, kidney, and intestinal samples were acquired by an MASm probe, an NMR semi-solid state method using the parameters described elsewhere (Saric *et al*, 2009).

Assignments of the spectral peaks were made from the literature (Nicholson *et al*, 1995; Coen *et al*, 2003; Li *et al*, 2008a, 2009; Saric *et al*, 2008) and confirmed through statistical total correlation spectroscopy (STOCSY) (Cloarec *et al*, 2005), and through standard two-dimensional NMR experiments conducted on selected samples, including correlation spectroscopy (Ernst *et al*, 1986), total correlation spectroscopy (Bax and Davies, 1985), and J-resolved NMR spectroscopy (Foxall *et al*, 1993). For selected brain samples, high-performance liquid chromatography (HPLC) was performed to isolate chemical components relating to unidentified-discriminatory metabolites with spectral regions at chemical shifts of δ 6.15 (doublet), δ 8.60 (singlet), δ 8.27 (singlet), and δ 4.02 (multiplet). For this purpose, fractions were separated using an Agilent 1100 HPLC with Eclipse XDB-C18 column, 5 μm, 4.6 × 150 mm (Agilent), attached to an Esquire 6000 mass spectrometer (MS; Bruker; Rheinstetten, Germany). An aliquot of 100 μl of brain extract was injected at a flow rate of 1 ml/min and signals were detected by UV at 214 nm and by MS in positive mode. A gradient of 98 % water to 2 % acetonitrile was used for the first 25 min and a standard gradient sequence was applied for the remaining 25 min. Fractions were collected over the first 8 min and then lyophilized and resuspended in D_2O for NMR analysis. Inosine, inosine monophosphate, inosine diphosphate, inosine triphosphate, adenosine, adenosine monophosphate, adenosine diphosphate, and adenosine triphosphate were confirmed by adding authentic standards purchased from Sigma Aldrich (Gilingham; Dorset, UK).

Data processing and analysis

The raw spectra were processed with an in-house developed MATLAB script to reduce phase and baseline distortions and manually calibrated to the lactate CH_3 signal at δ 1.33 (spectra of brain extracts, plasma, and tissue) or automatically to sodium 3-(trimethylsilyl) [2,2,3,3-$^2H_4$] propionate (TSP) at a spectral position δ 0.00 (urine and fecal water). The region containing the residual water resonance was removed to avoid any interference with the analysis (i.e. δ 4.55–5.40 in brain extracts, δ 4.2–8.0 in plasma, δ 4.63–5.15 in fecal extracts, δ 4.23–5.32 in urine, and a similar region of ∼δ 4.7–5.2 was removed in each tissue spectral dataset). Before statistical analysis, probabilistic quotient normalization was applied to all spectra and a peak alignment script was implemented in MATLAB to minimize chemical shift variation (Veselkov *et al*, 2009).

In a first step, PCA was applied to the processed spectral data to gain an overview of the degree of differentiation between infected and uninfected animals or inherent groupings in each tissue and biofluid spectral dataset (Eriksson *et al*, 2001). PCA reduces the multivariate data to a lower-dimensionality scores plot, without requiring any earlier class information and delivers a snapshot of the similarity between observations (i.e. brain spectra) based on the linear combination of the spectral components. In a second step, PLS-DA was applied, as a supervised method, which uses earlier information of class membership, and hence optimizes separation (Eriksson *et al*, 2001) and extraction of biomarkers associated with the infection.

O-PLS-DA is a further development of PLS-DA applied for optimal recovery of biomarkers (Trygg and Wold, 2002), and removes systematic variation unrelated to infection status through an orthogonal filter. The O-PLS-DA model was built by using an *X*-matrix containing all spectral information and a binary dummy matrix, as *Y*-determining class affiliation, for example infected or controls. Sevenfold cross-validation was applied (Bro *et al*, 2008) to validate the models and calculate the goodness of prediction Q^2. To validate the statistical power of the discriminatory metabolites, the *P*-values were calculated for each data point using 10 000 permutations and back projected to the O-PLS-DA plot, whereby regions that significantly differentiate infected from non-infected animals at a level of $P \leqslant 0.05$ are coded in red (Pitman, 1938).

For assessing the direct impact of the cerebral metabolic changes caused by *F. hepatica* infection, a further development of the STOCSY (Cloarec *et al*, 2005) and the statistical heterospectroscopy (Crockford *et al*, 2006) method has been applied between two data matrices whereby the selected regions occupied by each of the eight cerebral biomarkers were integrated in MATLAB and represent the *Y*-matrix. The spectral information of each other biological matrix (e.g. biofluids and all other tissues) constituted the second matrix (*X*) for calculating correlation structures between the spectral peaks and the integrated metabolite information. To reduce the display complexity and to avoid including artifacts and noise, spectral peaks were picked by applying a threshold of 100 × the s.d. calculated from the first 500 data points, which consist of noise only. A 10 000-fold permutation was embedded in the correlation script and only correlations with $P \leqslant 0.05$ are displayed.

Cytokine multiplex quantification

Plasma from five *F. hepatica*-infected rats and five uninfected rats from earlier NMR spectral preparation (e.g. 0.9 % saline (NaCl) in

D_2O:H_2O=1:1), over six different time points, were tested by a 'Mesoscale Multiplex Assay' (MS6000 Rat Demonstration 7-Plex Ultra-Sensitive kit, Meso Scale Discovery). The rat demonstration '7-Plex Ultra-Sensitivity kit' was used for this purpose, which includes IFN-γ, IL-1β, IL-4, IL-5, IL-13, KC/GRO, and TNF-α. Each sample was assessed using duplicates and split in 15 µl per well in a 96-well plate. The method was used according to the manufacturer's specifications (Meso Scale Discovery, Rat cytokine assays: Rat demonstration 7-Plex Ultra-Sensitive kit), with the exception of the incubation time, which was extended to 4 h to counteract the 1:1 dilution. An MSD Sector imager was used to read the plates (Meso Scale Discovery, Sector Imager 6000).

Supplementary information

Supplementary information is available at the *Molecular Systems Biology* website (http://www.nature.com/msb).

Acknowledgements

We thank Dr K Veselkov, S Robinette, and Dr I Yap for providing in-house software and G Calvert from Meso Scale Discovery for providing expertise on the cytokine assay. This study received financial support from the Swiss National Science Foundation to JS, JVL, JU (project no. PPOOB-102883 and PPOOB-119129), and JK (project no. PPOOA-114941), and from Chinese Academy of Sciences to YW (project no. KJCX2-YW-W11). Additional support was provided for JS by the Sir Henry Wellcome Fellowship (Wellcome Trust award number P23665).

Conflict of interest

The authors declare that they have no conflict of interest.

References

Ali EM (2008) *Fasciola gigantica*: purification and characterization of adenosine deaminase. *Exp Parasitol* **119:** 285–290

Bax A, Davies DG (1985) MLEV-17-based two-dimensional homonuclear magnetization transfer spectroscopy. *J Magn Reson* **65:** 355–360

Beckonert O, Keun HC, Ebbels TM, Bundy J, Holmes E, Lindon JC, Nicholson JK (2007) Metabolic profiling, metabolomic and metabonomic procedures for NMR spectroscopy of urine, plasma, serum and tissue extracts. *Nat Protoc* **2:** 2692–2703

Bell JD, Brown JC, Nicholson JK, Sadler PJ (1987a) Assignment of resonances for 'acute-phase' glycoproteins in high resolution proton NMR spectra of human blood plasma. *FEBS Lett* **215:** 311–315

Bell JD, Sadler PJ, Macleod AF, Turner PR, La Ville A (1987b) ^{1}H NMR studies of human blood plasma. Assignment of resonances for lipoproteins. *FEBS Lett* **219:** 239–243

Bro R, Kjeldahl K, Smilde AK, Kiers HA (2008) Cross-validation of component models: a critical look at current methods. *Anal Bioanal Chem* **390:** 1241–1251

Calder PC (2008) Polyunsaturated fatty acids, inflammatory processes and inflammatory bowel diseases. *Mol Nutr Food Res* **52:** 885–897

Calder PC (2009) Polyunsaturated fatty acids and inflammatory processes: new twists in an old tale. *Biochimie* **91:** 791–795

Cloarec O, Dumas ME, Craig A, Barton RH, Trygg J, Hudson J, Blancher C, Gauguier D, Lindon JC, Holmes E, Nicholson J (2005) Statistical total correlation spectroscopy: an exploratory approach for latent biomarker identification from metabolic ^{1}H NMR data sets. *Anal Chem* **77:** 1282–1289

Coen M, Lenz EM, Nicholson JK, Wilson ID, Pognan F, Lindon JC (2003) An integrated metabonomic investigation of acetaminophen toxicity in the mouse using NMR spectroscopy. *Chem Res Toxicol* **16:** 295–303

Crockford DJ, Holmes E, Lindon JC, Plumb RS, Zirah S, Bruce SJ, Rainville P, Stumpf CL, Nicholson JK (2006) Statistical heterospectroscopy, an approach to the integrated analysis of NMR and UPLC-MS data sets: application in metabonomic toxicology studies. *Anal Chem* **78:** 363–371

Eriksson L, Johansson E, Kettaneh-Wold N, Trygg J, Wikstrom C (2001) *Multi and Megavariate Data Analysis Part I: Basic Principles and Applications*. Umea, Sweden: Umetrics Academy

Ernst RRBG, Bodenhauser G, Wokaun A (1986) *Principles of Nuclear Magnetic Resonance in One and Two Dimensions*. Oxford: Clarendon

Fairweather I (2009) Triclabendazole progress report, 2005–2009: an advancement of learning? *J Helminthol* **83:** 139–150

Foxall PJ, Parkinson JA, Sadler IH, Lindon JC, Nicholson JK (1993) Analysis of biological fluids using 600 MHz proton NMR spectroscopy: application of homonuclear two-dimensional J-resolved spectroscopy to urine and blood plasma for spectral simplification and assignment. *J Pharm Biomed Anal* **11:** 21–31

Gounaris K (2002) Nucleotidase cascades are catalyzed by secreted proteins of the parasitic nematode *Trichinella spiralis*. *Infect Immun* **70:** 4917–4924

Hasko G, Kuhel DG, Nemeth ZH, Mabley JG, Stachlewitz RF, Virag L, Lohinai Z, Southan GJ, Salzman AL, Szabo C (2000) Inosine inhibits inflammatory cytokine production by a posttranscriptional mechanism and protects against endotoxin-induced shock. *J Immunol* **164:** 1013–1019

Hasko G, Sitkovsky MV, Szabo C (2004) Immunomodulatory and neuroprotective effects of inosine. *Trends Pharmacol Sci* **25:** 152–157

Holmes E, Loo RL, Stamler J, Bictash M, Yap IKS, Chan Q, Ebbels T, De Iorio M, Brown IJ, Veselkov KA, Daviglus ML, Kesteloot H, Ueshima H, Zhao L, Nicholson JK, Elliott P (2008a) Human metabolic phenotype diversity and its association with diet and blood pressure. *Nature* **453:** 396–400

Holmes E, Tsang TM, Tabrizi SJ (2006) The application of NMR-based metabonomics in neurological disorders. *NeuroRx* **3:** 358–372

Holmes E, Wilson ID, Nicholson JK (2008b) Metabolic phenotyping in health and disease. *Cell* **134:** 714–717

Keiser J, Utzinger J (2009) Food-borne trematodiases. *Clin Microbiol Rev* **22:** 466–483

Kreis R, Farrow N, Ross BD (1991) Localized ^{1}H NMR spectroscopy in patients with chronic hepatic encephalopathy. Analysis of changes in cerebral glutamine, choline and inositols. *NMR Biomed* **4:** 109–116

Lederberg J (2000) Infectious history. *Science* **288:** 287–293

Li JV, Holmes E, Saric J, Keiser J, Dirnhofer S, Utzinger J, Wang Y (2009) Metabolic profiling of a *Schistosoma mansoni* infection in mouse tissues using magic angle spinning-nuclear magnetic resonance spectroscopy. *Int J Parasitol* **39:** 547–558

Li JV, Wang Y, Saric J, Nicholson JK, Dirnhofer S, Singer BH, Tanner M, Wittlin S, Holmes E, Utzinger J (2008a) Global metabolic responses of NMRI mice to an experimental *Plasmodium berghei* infection. *J Proteome Res* **7:** 3948–3956

Li M, Wang B, Zhang M, Rantalainen M, Wang S, Zhou H, Zhang Y, Shen J, Pang X, Wei H, Chen Y, Lu H, Zuo J, Su M, Qiu Y, Jia W, Xiao C, Smith LM, Yang S, Holmes E *et al* (2008b) Symbiotic gut microbes modulate human metabolic phenotypes. *Proc Natl Acad Sci USA* **105:** 2117–2122

Li Z, Vance DE (2008) Phosphatidylcholine and choline homeostasis. *J Lipid Res* **49:** 1187–1194

Liaudet L, Mabley JG, Pacher P, Virag L, Soriano FG, Marton A, Hasko G, Deitch EA, Szabo C (2002) Inosine exerts a broad range of antiinflammatory effects in a murine model of acute lung injury. *Ann Surg* **235:** 568–578

Lim JH, Kim SY, Park CM (2007) Parasitic diseases of the biliary tract. *Am J Roentgenol* **188:** 1596–1603

Mabley JG, Rabinovitch A, Suarez-Pinzon W, Hasko G, Pacher P, Power R, Southan G, Salzman A, Szabo C (2003) Inosine protects against the development of diabetes in multiple-low-dose streptozotocin and nonobese diabetic mouse models of type 1 diabetes. *Mol Med* **9:** 96–104

Marcos LA, Terashima A, Gotuzzo E (2008) Update on hepatobiliary flukes: fascioliasis, opisthorchiasis and clonorchiasis. *Curr Opin Infect Dis* **21:** 523–530

Marquardt DL, Parker CW, Sullivan TJ (1978) Potentiation of mast cell mediator release by adenosine. *J Immunol* **120:** 871–878

Martin FPJ, Dumas ME, Wang Y, Legido-Quigley C, Yap IKS, Tang H, Zirah S, Murphy GM, Cloarec O, Lindon JC, Sprenger N, Fay LB, Kochhar S, van Bladeren P, Holmes E, Nicholson JK (2007) A top-down systems biology view of microbiome-mammalian metabolic interactions in a mouse model. *Mol Syst Biol* **3:** 112

Martin FPJ, Verdu EF, Wang Y, Dumas ME, Yap IKS, Cloarec O, Bergonzelli GE, Corthesy-Theulaz I, Kochhar S, Holmes E, Lindon JC, Collins SM, Nicholson JK (2006) Transgenomic metabolic interactions in a mouse disease model: interactions of *Trichinella spiralis* infection with dietary *Lactobacillus paracasei* supplementation. *J Proteome Res* **5:** 2185–2193

Minty A, Chalon P, Derocq JM, Dumont X, Guillemot JC, Kaghad M, Labit C, Leplatois P, Liauzun P, Miloux B (1993) Interleukin-13 is a new human lymphokine regulating inflammatory and immune responses. *Nature* **362:** 248–250

Nicholls AW, Mortishire-Smith RJ, Nicholson JK (2003) NMR spectroscopic-based metabonomic studies of urinary metabolite variation in acclimatizing germ-free rats. *Chem Res Toxicol* **16:** 1395–1404

Nicholson JK, Connelly J, Lindon JC, Holmes E (2002) Metabonomics: a platform for studying drug toxicity and gene function. *Nat Rev Drug Discov* **1:** 153–161

Nicholson JK, Foxall PJ, Spraul M, Farrant RD, Lindon JC (1995) 750 MHz ^{1}H and ^{1}H-^{13}C NMR spectroscopy of human blood plasma. *Anal Chem* **67:** 793–811

Nicholson JK, Holmes E, Wilson ID (2005) Gut microorganisms, mammalian metabolism and personalized health care. *Nat Rev Microbiol* **3:** 431–438

Nicholson JK, Lindon JC, Holmes E (1999) 'Metabonomics' understanding the metabolic responses of living systems to pathophysiological stimuli via multivariate statistical analysis of biological NMR spectroscopic data. *Xenobiotica* **29:** 1181–1189

Olde Damink SW, Deutz NE, Dejong CH, Soeters PB, Jalan R (2002) Interorgan ammonia metabolism in liver failure. *Neurochem Int* **41:** 177–188

Parshad VR, Guraya SS (1977) Comparative histochemical observations on the excretory system of helminth parasites. *Z Parasitenkd* **52:** 81–89

Pitman EJG (1938) Significance tests which may be applied to samples from any populations III. The analysis of variance test. *Biometrika* **29:** 322–335

Ribeiro JM, Francischetti IM (2003) Role of arthropod saliva in blood feeding: sialome and post-sialome perspectives. *Annu Rev Entomol* **48:** 73–88

Saric J, Li JV, Wang Y, Keiser J, Bundy JG, Holmes E, Utzinger J (2008) Metabolic profiling of an *Echinostoma caproni* infection in the mouse for biomarker discovery. *PLoS Negl Trop Dis* **2:** e254

Saric J, Li JV, Wang Y, Keiser J, Veselkov K, Dirnhofer S, Yap IKS, Nicholson JK, Holmes E, Utzinger J (2009) Panorganismal metabolic response modeling of an experimental *Echinostoma caproni* infection in the mouse. *J Proteome Res* **8:** 3899–3911

Schreiber G, Howlett G, Nagashima M, Millership A, Martin H, Urban J, Kotler L (1982) The acute phase response of plasma protein synthesis during experimental inflammation. *J Biol Chem* **257:** 10271–10277

Tilley SL, Wagoner VA, Salvatore CA, Jacobson MA, Koller BH (2000) Adenosine and inosine increase cutaneous vasopermeability by activating A(3) receptors on mast cells. *J Clin Invest* **105:** 361–367

Trygg J, Wold S (2002) Orthogonal projections to latent structures (OPLS). *J Chemom* **16:** 119–128

Tsang TM, Haselden JN, Holmes E (2009) Metabonomic characterization of the 3-nitropropionic acid rat model of Huntington's disease. *Neurochem Res* **34:** 1261–1271

Veselkov KA, Lindon JC, Ebbels TM, Crockford D, Volynkin VV, Holmes E, Davies DB, Nicholson JK (2009) Recursive segment-wise peak alignment of biological (1)H NMR spectra for improved metabolic biomarker recovery. *Anal Chem* **81:** 56–66

Wang Y, Utzinger J, Saric J, Li JV, Burckhardt J, Dirnhofer S, Nicholson JK, Singer BH, Brun R, Holmes E (2008) Global metabolic responses of mice to *Trypanosoma brucei brucei* infection. *Proc Natl Acad Sci USA* **105:** 6127–6132

Zaki AE, Ede RJ, Davis M, Williams R (1984) Experimental studies of blood brain barrier permeability in acute hepatic failure. *Hepatology* **4:** 359–363

Zaki AE, Wardle EN, Canalese J, Ede RJ, Williams R (1983) Potential toxins of acute liver failure and their effects on blood-brain barrier permeability. *Experientia* **39:** 988–991

Zeisel SH, Mar MH, Howe JC, Holden JM (2003) Concentrations of choline-containing compounds and betaine in common foods. *J Nutr* **133:** 1302–1307